Control of the magnetization in pre-patterned half-metallic $La_{0.7}Sr_{0.3}MnO_3$ nanostructures

J. Heidler,[1,2] J. Rhensius,[1,3,4] C. A. F. Vaz,[1,5,a)] P. Wohlhüter,[1,4] H. S. Körner,[1,4] A. Bisig,[4,5] S. Schweitzer,[4] A. Farhan,[3] L. Méchin,[6] L. Le Guyader,[2] F. Nolting,[2] A. Locatelli,[7] T. O. Menteș,[7] M. Á. Niño,[7] F. Kronast,[8] L. J. Heyderman,[3] and M. Kläui[1,4,5]

[1)] *SwissFEL, Paul Scherrer Institut, 5232 Villigen PSI, Switzerland*

[2)] *Swiss Light Source, Paul Scherrer Institut, 5232 Villigen PSI, Switzerland*

[3)] *Laboratory for Micro- and Nanotechnology, Paul Scherrer Institut, 5232 Villigen PSI, Switzerland*

[4)] *Fachbereich Physik, Universität Konstanz, Universitätsstraße 10, 78457 Konstanz, Germany*

[5)] *Institut für Physik, Johannes Gutenberg-Universität, 55099 Mainz, Germany*

[6)] *GREYC, UMR 6072, CNRS - ENSICAEN - UCBN, 6, Boulevard du Maréchal Juin, 14050 Caen Cedex, France*

[7)] *Elettra Sincrotrone Trieste S.C.p.A., 34149 Basovizza, Trieste, Italy*

[8)] *Helmholtz-Zentrum Berlin, Albert-Einstein-Straße 15, 12489 Berlin, Germany*

(Dated: 03.09.2012)

The evolution of the magnetization configurations in highly spin polarized $La_{0.7}Sr_{0.3}MnO_3$ (LSMO) thin film elements (20-60 nm in thickness) as a function of external magnetic field and temperature is studied by direct magnetic imaging using X-ray magnetic circular dichroism photoemission electron microscopy (XMCD-PEEM). The sample structuring is done via a pre-patterning process using a Cr mask layer. The LSMO grows amorphous on the Cr layer for the 20 nm thick film but polycrystalline at larger thicknesses. Temperature dependent studies allow for a direct comparison of the properties of the strained and unstrained LSMO regions on a single sample and show that the polycrystalline areas exhibit a higher T_C compared to the epitaxial areas. The single crystalline areas are largely magnetically decoupled from the matrix. The magnetic switching between domain states and domain wall spin structures is determined for LSMO ring elements of varying size and thickness. We find that the magnetic field values required to depin domain walls or to nucleate domains increase with decreasing ring width due to the increasing role of shape anisotropy and edge defects. Both transverse and vortex domain walls are stable spin configurations at room temperature and at zero field. In particular, we demonstrate that the desired domain wall type can be selected by applying an appropriate field sequence.

[a)]Corresponding author. Email: carlos.vaz@cantab.net

I. INTRODUCTION

Storage device applications based on concepts exploiting domain walls[1,2] require a detailed knowledge of the spin structure in magnetic nanostructures. The spin configuration should be stable at remanence and show reproducible magnetic field and current induced switching characteristics. For example, ring elements exhibit two stable magnetic domain states at remanence:[3–8] the 'onion' state, which is a high remanence state corresponding to a saturated state constrained by the topology of the element, and the 'vortex' state, which is a low remanence state with a flux closure spin structure that can be obtained upon applying a reverse magnetic field to an onion state. The onion state contains a head-to-head and a tail-to-tail domain wall which are usually transverse or vortex walls,[9] as determined by the interplay between exchange energy and shape anisotropy.[4,5] Hence, ring elements are ideally suited to study domain wall phenomena,[3,10] such as spin torque effects, or for application in spintronics. In this context, the optimally doped $La_{0.7}Sr_{0.3}MnO_3$ (LSMO) is a particularly interesting material since it is predicted to be half-metallic, with itinerant spin-up electrons and localized heavy spin-down electrons at the Fermi energy,[11] a measured spin polarization of nearly 100 %,[12] and a Curie temperature T_C up to 370 K.[13] However, fabrication of small structures in complex oxides is challenging. The high temperatures required for the growth of crystalline LSMO films exclude the structuring of the films using a lift-off technique with a polymer resist. Instead, the LSMO film can be structured after growth using focused ion beam (FIB),[14–16] Ar milling,[17] or electron beam lithography (EBL) and etching,[18] which, however, can induce defects during the patterning. An alternative approach, which we explore in this work, consists of using pre-patterned substrates to induce selective epitaxial growth of otherwise chemically homogeneous films.[19,20] LSMO grows epitaxially in a metallic, ferromagnetic phase on the bare substrate while in an amorphous, insulating, and non-magnetic phase on a Cr layer. To successfully incorporate LSMO nanostructures into spin-based electronic devices the ability to control and tune the magnetic domain structure is a key prerequisite. Magnetic switching in confined geometries, including in particular the domain wall switching properties, has not been comprehensively measured and analyzed for LSMO. Exchange, magnetostatic, magnetocrystalline, and magnetoelastic energies as well as substrate-induced strain govern the magnetic spin configuration of LSMO. At finite temperatures, thermal effects have an impact on the spin structure, which is an important

issue in modern data storage devices, and temperature dependent studies are necessary to investigate the interplay between competing micromagnetic energy terms and thus design a desired spin structure.

In this paper we examine the magnetization configurations and the switching behaviour of pre-patterned LSMO nanostructures. We demonstrate that for a given geometry distinct magnetic states and domain wall types can be controlled by the applied magnetic field. LSMO nanostructures (rings, squares, and wire elements) with various lateral dimensions are fabricated by a versatile pre-patterning technique that uses a Cr mask layer to define the epitaxial magnetic elements. Our results show that LSMO grows amorphous on the Cr layer for the 20 nm thick LSMO film but polycrystalline for thicker LSMO films. Surprisingly we find that the epitaxial magnetic elements are largely magnetically decoupled from the polycrystalline matrix. In the ring structures, both vortex and onion states are equilibrium states and the onion state exhibits stable transverse and vortex walls at room temperature. The dependence of the switching fields between the different domain configurations and the different domain wall spin structures on the ring geometry is determined. We find that in both rings and nanowires the magnetic field values needed to depin domain walls or to nucleate domains increase with decreasing width due to the enhanced role of shape anisotropy and edge defects. Temperature dependent studies allow for a direct comparison of the properties of the strained and unstrained LSMO regions on a single sample and show that the polycrystalline areas exhibit a higher T_C compared to the epitaxial areas.

II. SAMPLE FABRICATION AND EXPERIMENTAL METHODS

In this work, a 2 nm Cr mask layer was patterned on $SrTiO_3(001)$ (STO) substrates by EBL in order to define single crystalline LSMO elements in a non-epitaxial amorphous matrix. Subsequently, LSMO films, 20, 30, 40, 50, and 60 nm thick, were deposited by pulsed laser deposition from a stoichiometric target. The laser radiation energy of the KrF excimer laser (248 nm) was 220 mJ at a repetition rate of 3 Hz. The oxygen pressure was 0.35 mbar and the substrate was held at 720 °C during growth.[21] After growth, the film surface morphology was characterised by optical and atomic force microscopy (AFM). We find that while the thinnest LSMO film shows a large optical contrast difference between the areas with and without the Cr mask layer, the contrast in the thicker samples is much

weaker. FIG. 1 compares the LSMO surface morphology of the 20 nm (a) and of the 30 nm thick film (b) in a region containing both epitaxial and non-epitaxial LSMO as determined by AFM. The data shows that the epitaxial areas are much smoother, having an average roughness of approximately $\sigma = 0.5$ nm, than the areas with the Cr mask layer ($\sigma = 3 - 7$ nm). The magnetic characterization was carried out using X-ray magnetic circular dichroism photoemission electron microscopy (XMCD-PEEM),[22] which is a non-destructive, element sensitive technique for imaging magnetic domains. In XMCD-PEEM the total electron yield is proportional to the dot product of the magnetization $\mathbf{M}$ and the helicity $\mathbf{P}$ of the elliptically polarized monochromatic light from a synchrotron source.[22] Hence, the intensity difference between opposite helicities is visible as magnetic contrast. The PEEM measurements were performed at the Nanospectroscopy beamline at Elettra (Trieste, Italy),[23] at the SIM beamline at the Swiss Light Source (Villigen, Switzerland),[24] and at the beamline UE49-PGM-a at BESSY-II (Helmholtz Zentrum Berlin, Germany),[25] employing the XMCD effect at the Mn L_3 edge. If not stated otherwise, field-induced changes of the spin structure were imaged at remanence after applying *in situ* magnetic fields generated by an electromagnet on the sample holder. From the XMCD results, we find that the 20 nm LSMO sample showed charging effects upon x-ray exposure due to the insulating amorphous matrix, which were overcome by the deposition of a 3 nm thick conducting Cu layer. However no charging was observed for the thicker LSMO films; in addition, the PEEM images showed XMCD contrast for the LSMO films grown on the Cr mask layer, implying that the thicker films grow polycrystalline (metallic and ferromagnetic) on Cr. This is in agreement with the loss of optical contrast in thicker LSMO films and with the qualitative difference in the surface morphology for the LSMO grown on the Cr mask layer, as observed in the AFM data shown in FIG. 1. However, field-induced domain wall depinning experiments in rings and wires show, that the matrix and the nanostructured elements are largely magnetically decoupled from each other. In the following, domain wall depinning and displacement measurements concentrate on the 30 nm thick LSMO film, which combines the feasibility of high resolution imaging with the good magnetic definition of the structures. The polycrystalline area results in an increased edge roughness for the elements surrounded by the polycrystalline matrix.

III. RESULTS AND DISCUSSION

A. Magnetic field-induced transition between domain states and domain walls in ring elements

We consider first the spin structure of LSMO ring elements as a function of width and applied magnetic field. While the literature already reports switching phase diagrams as a function of the geometrical parameters for Permalloy (NiFe) and Co ring structures,[4,5,7] no such data is available for LSMO thin film elements. Since PEEM images allow one to identify the domain configuration of the ring as a function of magnetic field as well as the domain wall types present, domain wall transitions are included in the systematic study, which was not determined previously in the studies on 3d metal structures. In FIG. 2 we show PEEM images showing the transformation of domain states and domain walls for a 1.5 μm wide ring of 30 nm thickness. In FIG. 2(a) the magnetization is initially in an onion state after applying an in-plane magnetic field of -13.00 mT and exhibits transverse domain walls, one head-to-head and one tail-to-tail. Next, an increasing reverse field is applied to the sample. At +2.60 mT, one domain wall depins and moves until the two walls annihilate, resulting in a vortex state (FIG. 2(c)). This state remains stable up to +3.56 mT, where two vortex walls are nucleated to create the reversed onion state (FIG. 2(d)). FIG. 2 also displays domain wall transformations that take place: At 2.52 mT one transverse wall transforms into a vortex wall (FIG. 2(a,b) highlighted with a circle). For clarity, the schematic of the spin structure of the transverse and vortex wall and the resulting contrast are depicted in FIG. 2(f) and (g), respectively. At 6.60 mT, one of the vortex walls in the reversed onion state transforms into a transverse wall by expelling the vortex core (FIG. 2(d,e) highlighted with a circle). These results show that for a given ring width we can selectively generate both wall types at zero field by applying a suitable magnetic field. Next, we study the domain state transitions in order to understand the underlying statistical and geometrical dependences. The transition between the onion and the vortex state is based on the depinning of one of the domain walls, which is a stochastic process that depends on local pinning sites and thermal activation.[7] The dependence of the vortex state transitions on the applied magnetic field was systematically studied for arrays of rings with widths ranging from 0.15 μm to 1.8 μm in a 30 nm thick LSMO film (FIG. 3(a)). The fraction of switched states (given in %) is plotted

as a function of the applied magnetic field. For the widest elements (width of 1.8 μm, open triangles), the onion state already switches into the vortex state at a field slightly above 1 mT. This is close to the coercive field of the continuous film, as determined on a large epitaxial area from superconducting quantum interference device (SQUID) magnetometry measurements. In the narrowest rings (open circles) the onion state remains stable up to fields of 7.00 mT. In general, the switching field increases continuously with decreasing ring width. For a given ring width the field values for the transition are spread in a range over 1 mT, which indicates that the transition is determined not only by the geometry of the element but is also influenced by random pinning. After the transition from an onion to a vortex state, a second transition from the vortex state to a reversed onion state occurs upon further increase of the magnetic field. The corresponding dependence of the transition from the vortex to the reversed onion state on the magnetic field is shown in FIG. 3(b) for different ring widths. For the 1.8 μm wide rings (open triangles), the reversed onion state is reached at a magnetic field of 3.60 mT. Rings with the smallest widths, 0.15 μm, switch to the reversed onion state at magnetic fields of 8.00 mT (open circles). Again, the field values of the transition for a given ring width are spread over a range of 1 mT. Also here, the magnitude of the switching field increases continuously with decreasing ring width. This is in line with the findings of previous domain state switching studies in Co and Permalloy.[4,5,7] From this data, the mean switching field for every ring geometry is determined by extracting the field at which 50% of the rings have switched. The resulting distribution is presented in FIG. 3(c). Open circles mark the transition from an onion state to the vortex state, filled circles mark the transition to the reversed onion state. In both onion to vortex and vortex to reversed onion state transitions, the switching field increases with decreasing ring width. This is in line with experiments performed on the switching behaviour of Co rings[5,26] and can be attributed mostly to the stronger pinning from the relatively larger edge roughness in narrower elements. For the onion to vortex transition this means that, in narrow elements, higher fields are required to depin one domain wall that annihilates the second domain wall. For the vortex to the reversed onion state transition the switching process involves the nucleation of a reverse domain at the edge of the ring. Since the nucleation is caused by twisting of the spins, it is less likely to occur in narrower elements, where the spins are more strongly aligned due to the increased shape anisotropy.[27] For narrow elements, the two switching fields (onion to vortex state, vortex to the reversed onion state) nearly

equalize. A possible explanation could be the pinning at the edge of the ring, which prevents the depinning of a domain wall (which triggers the onion to vortex state transition), while the vortex state annihilation is not as sensitive to the presence of edge defects. These results show that the patterning method and the material's properties strongly influence the nature of the magnetic reversal. FIG. 3(c) also shows the dependence of the domain wall transformation on the applied magnetic field and ring width: open triangles mark the domain wall transition from a transverse to a vortex wall, while filled triangles mark transitions from a vortex to a transverse wall. Before the domain state switches from the onion state into the vortex state, some of the transverse domain walls transform into vortex walls. We observe that the first transition from a transverse to a vortex wall (open triangles) appears approximately at half the depinning field of the domain wall (open circles). For Permalloy and Co usually one or the other domain wall type is stable at remanence depending on the ring geometry parameters and the field history.[28,29] Calculations regarding the stability of domain wall types in nanostructures as a function of thickness and width show that transverse walls are more likely to be found in thin films.[9,30] The stray field constitutes the main energy contribution and increases quadratically with film thickness. On the other hand, the vortex core of a vortex wall is highly energetic due to the exchange interaction between strongly twisted spins. As the exchange energy increases linearly with thickness, vortex walls are the stable configuration in thick film structures. For a constant thickness there is a transition from transverse to vortex walls with increasing ring width, as the stray field energy of the transverse wall increases more strongly with width than the exchange energy. As a consequence, for a given geometry, the domain wall spin structure is fixed. Interestingly, the pre-patterned LSMO film allows for the stabilization of both transverse walls and vortex walls in all these ring elements at room temperature. The observation of transverse walls can be attributed to the edge-pinning in the LSMO films. There exist not only local pinning sites within the epitaxial nanostructured regions, but the surrounding polycrystalline boundary can induce pinning at the edge (see also section III C), which can stabilize the transverse domain walls. After the vortex state transforms into the reversed onion state, mostly vortex domain walls are present. The filled triangle symbols in FIG. 3(c) show that the vortex walls in wide elements switch to transverse walls at lower fields than those in the narrow elements. The transition from vortex to transverse walls proceeds by the annihilation of the vortex core. The vortex core experiences a higher repulsion from the

wire edge for narrower ring widths. Therefore the switching requires larger fields in narrow rings, whereas for elements above 0.4 μm, the size dependence becomes less pronounced.

B. Field-induced domain wall depinning and displacement in wire structures

For experiments examining the displacement of domain walls, nanowires are a better suited geometry than rings, since In the latter, the displacement is limited to the size of the ring and the two walls of the onion state can interact, resulting, for instance, in the annihilation and the formation of the vortex state as discussed above. Thus, we study field-induced spin structure changes in magnetic nanowires with domain walls. This is also interesting for applications based on domain wall displacement, where reproducible domain wall motion and low depinning fields are required. In this experiment, fields are applied along the [100] direction in 30 nm thick zig-zag wires with widths varying between 0.5 and 2.5 μm The patterned wires are directly connected to a large LSMO domain wall nucleation pad. Prior to magnetic imaging, the sample was magnetized in the opposite (negative) field direction. The magnetization in the nucleation pad is found to switch at a positive field of approximately 1 mT. The injection field necessary to move a domain wall inside the wire is higher than this value. FIG. 4 shows the influence of an increasing magnetic field for two 1.5 μm wide zig-zag wires. At an applied field of 1.30 mT (FIG. 4(a)), a vortex domain wall is present in each wire. By further increasing the field to 1.50 mT (FIG. 4(b)), the domain walls depin and move along the field direction. We observe that local pinning sites dominate the propagation. In FIG. 4(c) at a magnetic field of 2.30 mT the wall in the left wire already moved out of the field of view, while the vortex wall of the right wire is still stabilized at a pinning site close to the pad. The depinning field corresponding to the value where approximately four out of eight wires for every wire width have switched, is plotted as a function of different wire geometries in FIG. 4(d), showing that smaller wire dimensions require larger magnetic fields to depin the domain walls analogous to the observed domain wall depinning in rings (see section III A). The increase in the depinning field with decreasing width of the wire has been previously observed in Permalloy by Adeyeye et al.,[31,32] where a crossover from an interacting wire array to isolated wires is found for $s/w \geq 1$, where w is the element width and s the wire spacing. For the case of isolated wires a $1/w$ dependence for the depinning field was found. The $1/w$ dependence of the depinning field in LSMO

domain walls (FIG. 4(d)) is in line with these findings. The spacing s between the LSMO wires is relatively large, so no direct magnetostatic coupling is expected. The depinning sequence in FIG. 4 is particularly interesting, since it shows that despite the presence of a polycrystalline matrix in between the wires, the domain walls move independently from each other and there is no strong direct coupling between the epitaxial LSMO wires.

C. Magnetic behaviour near the Curie temperature

The magnetic behaviour of the epitaxial and polycrystalline areas as a function of temperature is especially interesting, as it is directly related to the strain imposed from the substrate. Here, the thermally activated change and nucleation of domains in square elements in a 60 nm thick LSMO sample is studied as the temperature is slowly increased from 334 K to above T_C. In order to circumvent the uncertainty of the thermocouple used to measure the specimen temperature in the PEEM (we estimate an error of about 5 K around room temperature, but relative changes can be determined with high accuracy), SQUID measurements on a 30 nm thick LSMO film were used to calibrate the temperature scale for the XMCD data. The heating sequence of a square element with an edge size of 12 μm is shown in FIG. 5. In (a), the element is in a multidomain state with relatively large domains. The grains of the surrounding polycrystalline material define the edge roughness, which is visible in the small distortion of the magnetization at the edge of the element. The XMCD contrast is high and is present also in the surrounding grains, which means that they are also ferromagnetic. By increasing the temperature to 335 K, the domain boundaries in the element show reduced contrast (FIG. 5(b)). At 335.5 K (FIG. 5(c)), the contrast in the central part of the patterned element is strongly reduced and appears uniformly grey. Only the area in the epitaxial element close to the edges shows some contrast and also the polycrystalline area around the element remains ferromagnetic. This could be attributed to a small coupling that stabilizes the domain state at the border of the epitaxial element. At a temperature of 335.8 K (see FIG. 5(d)) the Curie temperature for the epitaxially grown area is reached, as indicated by the vanishing contrast in the square element, whereas a weak magnetic contrast remains in the surrounding grains. Hence, we find that T_C for the polycrystalline LSMO is slightly higher than that of epitaxial LSMO. This is in agreement with previous results showing that biaxial strain causes a reduction of T_C in LSMO films[33–36]

with respect to the bulk value.[13,37] Here, the epitaxially grown LSMO experiences a tensile in-plane strain due to the lattice mismatch at the interface with the STO substrate. The LSMO grown on the Cr layer is polycrystalline, where each crystallite is expected to be fully relaxed with a T_C near the bulk value. These results provide a direct demonstration of the effect of strain on the magnetic critical temperature of LSMO, since the sample has a homogeneous temperature within the field of view. FIG. 5(d) also shows a slightly increased T_C at the element boundaries within the epitaxially grown area compared to the inner part of the square. At 339 K (FIG. 5(e)), the contrast vanishes completely. When the sample is cooled down again, the contrast first returns in the polycrystalline area (FIG. 5(f)). As cooling is continued, very small domains form in the square element (FIG. 5(g)). Here, the randomly distributed spins of the paramagnetic phase start to freeze and small domains form independently. As the temperature decreases another 0.5 K, the small domains merge into bigger domains, in order to minimize the domain wall energy (FIG. 5(h)). Though we observe a small magnetic interaction with the grains of the polycrystalline matrix at the border of the epitaxial nanostructures close to the transition temperature (FIG. 5(c)), this effect disappears for only 0.3 K higher temperature (FIG. 5(d)) highlighting that the coupling is weak, in line with the results from section III B.

D. Conclusions

In summary, we investigated the magnetic properties of LSMO films pre-patterned into small elements using a Cr mask prior to the LSMO growth. The LSMO is found to grow amorphous on top of a Cr layer for thin films (20 nm) and polycrystalline for thicker films (30-60 nm). The evolution of the magnetization configuration in the LSMO thin film elements was studied as a function of external magnetic field and temperature. Temperature dependent measurements show that the T_C of the epitaxial areas is slightly lower than the T_C of the polycrystalline areas due to the substrate-induced strain. The single crystalline areas are largely magnetically decoupled from the polycrystalline areas, which act only as a source of pinning. We find that, for ring elements, both transverse and vortex walls are stable spin configurations at room temperature and we can set the domain wall type by applying an appropriate field sequence. Our results show that the magnetic field values required to depin domain walls or nucleate domains increase with decreasing width of the

rings and are in qualitative agreement with the findings in 3d metals, indicating that the properties of the nanostructure are mainly governed by their geometry.

ACKNOWLEDGMENTS

Part of this work was performed at the Swiss Light Source, Paul Scherrer Institut, Villigen, Switzerland and at Elettra, Sincrotrone Trieste, Italy as well as at the Helmholtz-Zentrum Berlin, Germany. This work was funded by EUs 7th Framework Programme IFOX (NMP3-LA-2010 246102), MAGWIRE (FP7-ICT-2009-5 257707), the European Research Council through the Starting Independent Researcher Grant MASPIC (ERC-2007-StG 208162), the Swiss National Science Foundation, and the DFG.

REFERENCES

[1]R. Cowburn, US Patent (2007), WO/2007/132174.

[2]S. S. P. Parkin, M. Hayashi, and L. Thomas, Science **320**, 190 (2008).

[3]J. Rothman, M. Kläui, L. Lopez-Diaz, C. A. F. Vaz, A. Bleloch, J. A. C. Bland, Z. Cui, and R. Speaks, Phys. Rev. Lett. **86**, 1098 (2001).

[4]M. Kläui, C. A. F. Vaz, L. J. Heyderman, U. Rüdiger, and J. A. C. Bland, J. Magn. Magn. Mater. **290-291**, 61 (2005).

[5]Y. G. Yoo, M. Kläui, C. A. F. Vaz, L. J. Heyderman, and J. A. C. Bland, Appl. Phys. Lett. **82**, 2470 (2003).

[6]F. J. Castaño, C. A. Ross, A. Eilez, W. Jung, and C. Frandsen, Phys. Rev. B **69**, 144421 (2004).

[7]M. Kläui, C. A. F. Vaz, J. A. C. Bland, E. H. C. P. Sinnecker, A. P. Guimarães, W. Wernsdorfer, G. Faini, E. Cambril, L. J. Heyderman, and C. David, Appl. Phys. Lett. **84**, 951 (2004).

[8]S. P. Li, D. Peyrade, M. Natali, A. Lebib, Y. Chen, U. Ebels, L. D. Buda, and K. Ounadjela, Phys. Rev. Lett. **86**, 1102 (2001).

[9]Y. Nakatani, A. Thiaville, and J. Miltat, J. Magn. Magn. Mater. **290-291**, 750 (2005).

[10]F. J. Castaño, C. A. Ross, C. Frandsen, A. Eilez, D. Gil, H. I. Smith, M. Redjdal, and F. B. Humphrey, Phys. Rev. B **67**, 184425 (2003).

[11]J. M. D. Coey and M. Venkatesan, J. Appl. Phys. **91**, 8345 (2002).

[12]J. H. Park, E. Vescovo, H. J. Kim, C. Kwon, R. Ramesh, and M. Venkatesan, Nature **392**, 794 (1998).

[13]G. H. Jonker and J. H. van Santen, Physica **16**, 337 (1950).

[14]Y. Takamura, R. V. Chopdekar, A. Scholl, A. Doran, J. A. Liddle, B. Harteneck, and Y. Suzuki, Nano Lett. **6**, 1287 (2006).

[15]J. S. Bettinger, R. V. Chopdekar, B. L. Mesler, A. Chain, D. Doran, E. Anderson, A. Scholl, and Y. Suzuki, Mater. Res. Soc. Symp. Proc. **1256**, N13 (2010).

[16]J. Rhensius, C. A. F. Vaz, A. Bisig, S. Schweitzer, J. Heidler, H. S. Körner, A. Locatelli, M. A. Niño, M. Weigand, L. Méchin, F. Gaucher, E. Goering, L. J. Heyderman, and M. Kläui, Appl. Phys. Lett. **99**, 062508 (2011).

[17]M. Kubota, Appl. Phys. Lett. **91**, 182503 (2007).

[18]G. Bridoux, J. Barzola-Quiquia, F. Bern, W. Böhlmann, I. Vrejoiu, M. Ziese, and P. Esquinazi, Nanotechnology **23**, 085302 (2012).

[19]S. P. Li, W. S. Lew, J. A. C. Bland, L. Lopez-Diaz, M. Natali, C. A. F. Vaz, and Y. Chen, Nature **415**, 600 (2002).

[20]C. A. F. Vaz, Y. Segal, J. Hoffman, F. J. Walker, and C. H. Ahn, J. Vac. Sci. Technol. B **28**, C5A6 (2010).

[21]P. Perna, C. Rodrigo, E. Jiménez, F. J. Teran, N. Mikuszeit, L. Méchin, J. Camarero, and R. Miranda, J. Appl. Phys. **110**, 013919 (2011).

[22]J. Stöhr, Y. Wu, B. D. Hermsmeier, M. G. Samant, G. R. Harp, S. Koranda, D. Dunham, and B. P. Tonner, Science **259**, 658 (1993).

[23]A. Locatelli, S. Cherifi, S. Heun, M. Marsi, K. Ono, A. Pavlovska, and E. Bauer, Surf. Rev. Lett. **9**, 171 (2002).

[24]U. Flechsig, J. Als-Nielsen, A. Jaggi, J. Krempaský, P. Oberta, S. Spielmann, and J. F. van der Veen, AIP Conference Proceedings **1234**, 653 (2010).

[25]F. Kronast, J. Schlichting, F. Radu, S. K. Mishra, T. Noll, and H. A. Dürr, Surface and Interface Analysis **42**, 1532 (2010).

[26]M. Kläui, L. Lopez-Diaz, J. Rothman, C. A. F. Vaz, J. A. C. Bland, and Z. Cui, J. Magn. Magn. Mater. **240**, 7 (2002).

[27]L. Lopez-Diaz, J. Rothman, M. Kläui, and J. A. C. Bland, IEEE Trans. Magn. **36**, 3155 (2000).

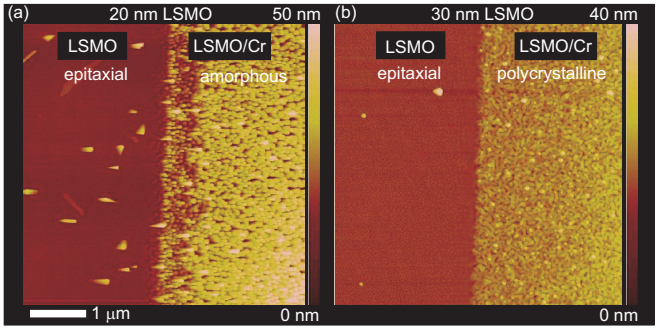

FIG. 1. (Color online) AFM images of the 20 nm (a) and the 30 nm (b) thick LSMO film. The field of view shows a bare LSMO/$SrTiO_3$ region to the left and a LSMO/Cr/$SrTiO_3$ region to the right.

[28]M. Kläui, Journal of Physics: Condensed Matter **20**, 313001 (2008).

[29]M. Kläui, C. A. F. Vaz, J. A. C. Bland, L. J. Heyderman, F. Nolting, A. Pavlovska, E. Bauer, C. Cherifi, and A. Locatelli, Appl. Phys. Lett. **85**, 4167 (2004).

[30]R. D. McMichael and M. J. Donahue, IEEE Trans. Magn. **33**, 4167 (1997).

[31]A. O. Adeyeye, J. A. C. Bland, C. Daboo, J. Lee, U. Ebels, and H. Ahmed, J. Appl. Phys. **79**, 6120 (1996).

[32]A. O. Adeyeye, J. A. C. Bland, C. Daboo, and D. G. Hasko, Phys. Rev. B **56**, 3265 (1997).

[33]A. J. Millis, T. Darling, and A. Migliori, J. Appl. Phys. **83**, 1588 (1998).

[34]F. Tsui, M. C. Smoak, T. K. Nath, and C. B. Eom, Appl. Phys. Lett. **76**, 2421 (2000).

[35]H. Röder, J. Zang, and A. R. Bishop, Phys. Rev. Lett. **76**, 1356 (1996).

[36]A. J. Millis, Nature **392**, 147 (1998).

[37]A. Urushibara, Y. Moritomo, T. Arima, A. Asamitsu, G. Kido, and Y. Tokura, Phys. Rev. B **51**, 14103 (1995).

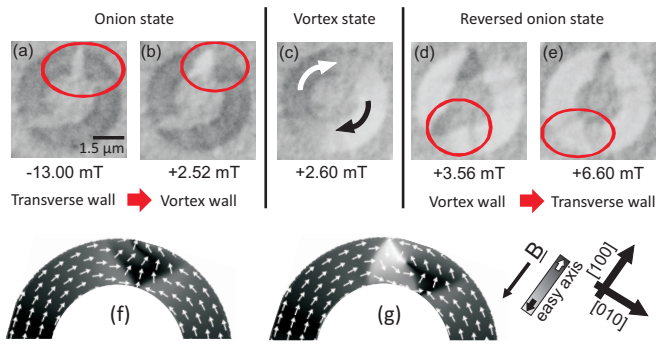

FIG. 2. (Color online) (a-e) XMCD-PEEM images of a 1.5 μm wide and 30 nm thick ring element as a function of the applied magnetic field. (f) and (g) show schematics of the spin structure of a transverse wall and a vortex wall, respectively.

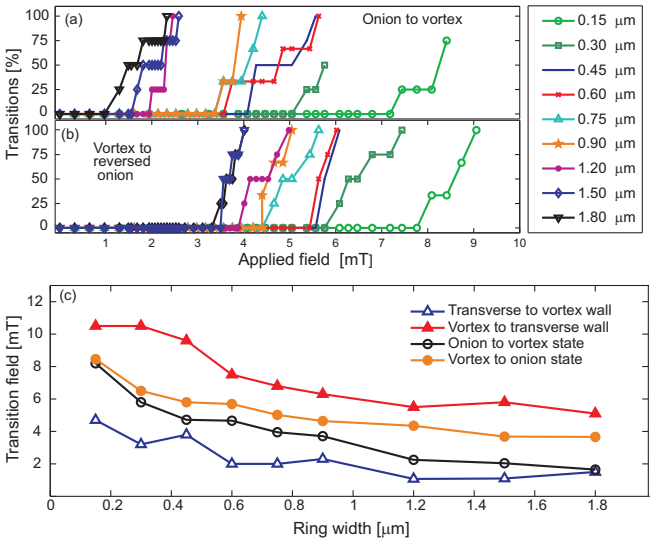

FIG. 3. (Color online) Transition from (a) the onion to the vortex state and (b) the vortex to the reversed onion state for an array of LSMO rings of 30 nm thickness with widths ranging from 0.15 μm to 1.80 μm (lines are guides to the eye). (c) Switching field dependence between vortex and onion states (circles) as well as domain wall transformations (triangles) as a function of ring width.

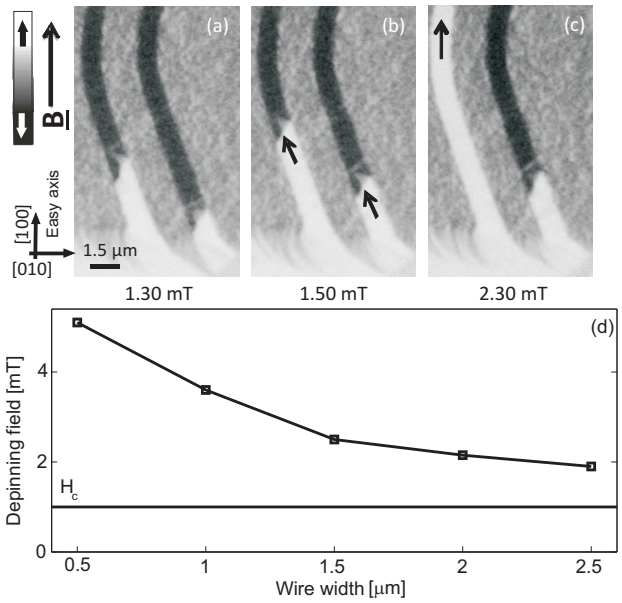

FIG. 4. (a,b,c) XMCD-PEEM images showing the field-induced displacement of domain walls in 1.5 μm wide and 30 nm thick LSMO wires with increasing magnetic field. (d) Depinning field for different wire widths in 30 nm LSMO wires (line is a guide to the eye). The coercive field H_C of the continuous LSMO film is indicated by the horizontal line.

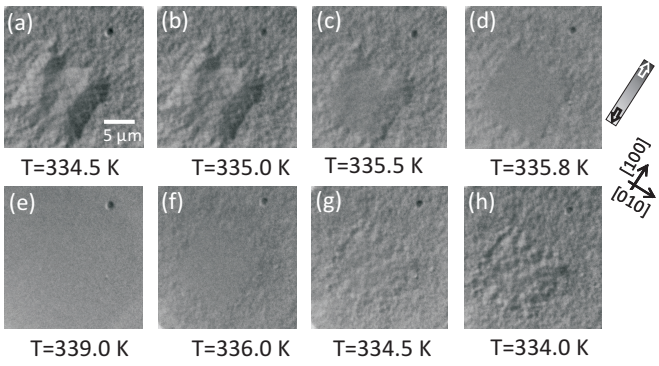

FIG. 5. XMCD images taken on a 60 nm thick LSMO film around T_C for a epitaxial square element surrounded by a polycrystalline matrix.